EPR of VO^{2+}-doped $K_2C_2O_4 \cdot H_2O$: Forbidden hyperfine transitions

Sushil K. Misra and Changlu Wang*
Physics Department, Concordia University, 1455 de Maisonneuve Boulevard West, Montreal, Quebec, Canada H3G 1M8
(Received 22 August 1988)

Detailed X-band EPR measurements on a single crystal of VO^{2+}-doped $K_2C_2O_4 \cdot H_2O$ have been carried out at 295, 80, 42, and 4.2 K. In addition to the allowed transitions, strong nominally forbidden hyperfine (hf) transitions were observed. Out of the two lines of each of the expected forbidden doublets, only one line was of sufficient intensity to be observed in the EPR spectra, at all orientations of the external magnetic field. The relative intensities of the various forbidden hf lines, and the angular variations of the intensities of the allowed and forbidden hf lines have been well explained theoretically to be due to the hyperfine interaction. The principal values of the $\underline{g}^2$ and $\underline{A}^2$ tensors of VO^{2+}, as well as the orientations of their principal axes, are evaluated from the positions of the allowed lines, by use of a least-squares-fitting procedure, in which all allowed hf line positions, observed for the external magnetic field orientation in three mutually perpendicular planes, are simultaneously fitted. The principal values and direction cosines of the principal axes of the tensor $\underline{Q}$ are evaluated from the forbidden hf line positions, by another least-squares-fitting procedure. The asymmetry parameter has been estimated from the principal values of the tensor $\underline{Q}$. The present study confirms that the VO^{2+} ions enter interstitially, displacing two K^{2+} ions; the orientations of the various VO^{2+} molecules (V^{4+}—O^{2-} bonds) are close to either the quasitwofold axis of the distorted coordination octahedron formed by four oxygen ions and two water molecules, or the $K(1)^+$-$K(2)^+$, direction.

I. INTRODUCTION

Numerous EPR studies on VO^{2+}-doped single crystals have been reported to date.[1,2] However, most of these have been confined to the observation of allowed hyperfine (hf) transitions $\Delta M = \pm 1$, $\Delta m = 0$, where M and m are, respectively, the electronic and nuclear magnetic quantum numbers. It is not possible to evaluate the quadrupole tensor precisely from the allowed line positions, since the eigenvalue differences between the relevant energy levels do not depend upon the quadrupole tensor in the first order of perturbation. However, the forbidden-hf-transition line positions do depend on the quadrupole tensor, and, as shown below, its components can be evaluated from the forbidden-hf-transition line positions. Forbidden hf transitions ($\Delta M = \pm 1$, $\Delta m = \pm 1$) for VO^{2+} have been observed only in relatively few systems[3-5] due to their weaker intensity. The detection of forbidden lines in the EPR spectra becomes even more difficult when there are other physically inequivalent VO^{2+} complexes present, due to overlap of spectra. Misra and Upreti[1,2] have discussed various mechanisms giving rise to forbidden hf transitions in the EPR of iron-group ions.

Angular variations of the intensities of the forbidden lines of Mn^{2+} in some single crystals, for the configuration where the excitation (microwave) field has a nonzero component parallel to the external Zeeman field, have been previously reported.[6-9] However, their calculations were made for the simple case when the $\underline{g}^2$ ($\equiv \underline{g}^T \cdot \underline{g}$, where T denotes transpose) tensor is isotropic and the $\underline{A}^2$ ($\equiv \underline{A}^T \cdot \underline{A}$) tensor is either isotropic, or axially symmetric.

EPR studies on VO^{2+}-doped single crystal of potassium oxalate monohydrate $K_2C_2O_4 \cdot H_2O$ (hereafter POM) have been previously reported by Jain.[10] However, his measurements were confined to room temperature (RT) only and the forbidden hf transitions were not observed. Furthermore, the $\underline{g}^2$ and $\underline{A}^2$ tensors were assumed to be coincident for the evaluation of spin-Hamiltonian parameters from the line positions, and their values were estimated only for one VO^{2+} complex. He concluded that the VO^{2+} ion enters the crystal lattice in two identical, but differently oriented, interstitial sites.

The present paper reports detailed X-band EPR studies on VO^{2+}-doped POM single crystals from RT down to liquid-helium temperature (LHT). In addition to observing the allowed hf transitions, particular attention has here been focused on the observation of forbidden hf transitions. This is accomplished by choosing the orientation of the external magnetic field with respect to the excitation field such that the excitation field has nonzero components both along and perpendicular to the Zeeman field. The intensity expressions for these transitions, assuming that the $\underline{g}^2$ and $\underline{A}^2$ tensors are both anisotropic and noncoincident, and that the direction of the excitation field makes an arbitrary angle with the direction of the external magnetic field, have been derived by taking the time-dependent excitation Hamiltonian into account. The allowed-line-position data have been used to evaluate the components of the $\underline{g}^2$ and $\underline{A}^2$ tensors by the method of least-squares fitting, using second-order perturbed eigenvalues.[11] On the other hand, the quadrupole tensor $\underline{Q}$ has been estimated from the forbidden-hf-transition line positions. The direction cosines of the principal axes of the $\underline{g}^2$ tensor have been used to deduce the orientations of the V^{4+}-O^{2-} bonds in the POM lattice.

II. CRYSTAL STRUCTURE AND SAMPLE PREPARATION

The POM crystal is characterized by monoclinic symmetry with the unit-cell dimensions $a = 9.210$, $b = 6.165$, $c = 10.660$ Å, and $\beta = 110.9°$, belonging to the space group $C2/c$.[12,13] The site symmetries at the potassium and water molecules are $C1$ and $C2$, respectively. The unit cell contains four formula units. The potassium ion is surrounded by eight oxygen atoms, out of which seven belong to four oxalate groups and one to a water molecule. The K-O distances range anywhere from 2.745 to 3.015 Å. Figure 1 shows the projection of the POM structure onto the (010) plane.

Blue single crystals of POM, doped with VO^{2+}, were grown at room temperature by slow evaporation from saturated aqueous solution of potassium oxalate containing 1% (by weight) of vanadyl sulfate dihydrate. The most-developed faces in these crystals were found to be the (001), (111), and ($\bar{1}11$) faces. See Fig. 2 for the growth habit of the crystal. A crystal of size $1.0 \times 1.0 \times 2.5$ mm^3 was chosen for the present measurements.

III. EXPERIMENTAL ARRANGEMENT AND DETAILS OF SPECTRA

A Varian V4502 X-band spectrometer was used for the present observations. The magnetic field for the spectra was calibrated with a Bruker (B-NM20) Gaussmeter; the line position determined from the graph had an accuracy of 0.5 G. The temperature was varied by the use of a heater resistor inside the liquid-helium cryostat. For angular-variation studies, the excitation field and the crystal sample were kept fixed while the external magnetic field was rotated.

EPR spectra were recorded in three mutually perpendicular planes, defined by the axes X, Y, and Z. In each plane, the external magnetic field orientation was varied at 5° intervals. The ZX plane was chosen parallel to the {001} face of the crystal; the orientation of the Z and X axes relative to the a and b axes of the crystal are exhibited in Fig. 2.

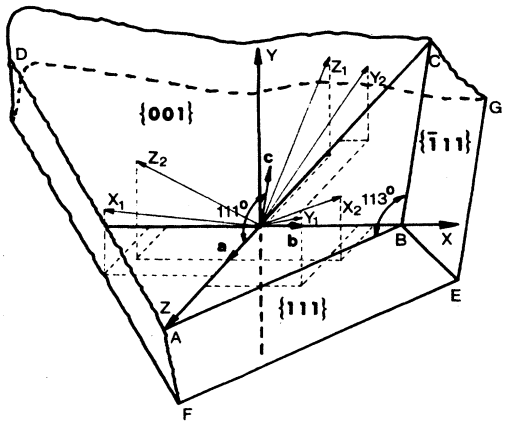

FIG. 2. Crystal-growth habit of POM, *ABCD*, *ABEF*, and *BCGE* are, respectively, the (001), (111), and ($\bar{1}11$) planes. The directions of the unit-cell vectors **a**, **b**, and **c** are indicated, where **a** and **b** are in the {001} plane. The orientations of the laboratory axes X, Y, and Z with respect to the crystal faces have been indicated. The Z axis is coincident with **a**, while the X axis is coincident with **b**. The principal axes of the g matrix of the two VO^{2+} complex (X_1, Y_1, Z_1) and (X_2, Y_2, Z_2) are also indicated.

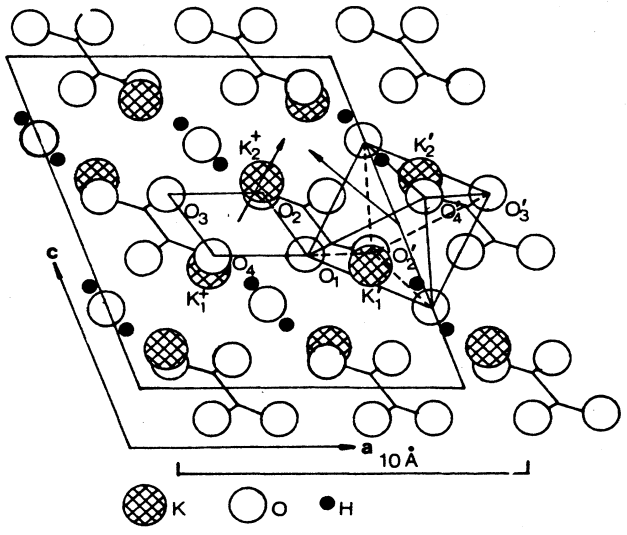

FIG. 1. Projection of the POM crystal structure on the {010} plane. Note that O_1' and O_1 are the same.

Angular variation of the EPR spectra, as observed for rotation of the external magnetic field in any of the XY, YZ, and ZX planes, revealed the presence of two different sets of eight allowed-hf-transition lines $(\frac{1}{2}, m \leftrightarrow -\frac{1}{2}, m)$, and two sets of seven forbidden-hf-transition lines $(\frac{1}{2}, m \leftrightarrow -\frac{1}{2}, m+1)$ for VO^{2+} at all temperatures. (For more details, see Sec. V.) One of the hf-forbidden sets was so weak that it could be observed at only a very few orientations of the external magnetic field. The intensities of the two allowed hf sets of lines were found to be, generally, in the ratio 6:1. This indicates that the two sites (referred to as I and II) which VO^{2+} ions can occupy, are populated approximately in the ratio 6:1. The more intense set of seven forbidden-hf-transition lines corresponds to the VO^{2+} complex occupying site I. It was found that, as the orientation of the external magnetic field gets closer to the direction of the crystallographic c axis, the allowed-hf-transition lines of site I begin to become wider due to superhyperfine splitting, with a corresponding decrease in their peak-to-peak heights; the maximum width is attained when the external magnetic field is parallel to the crystallographic c axis. Figure 3 shows the spectra obtained at an angle $\theta = 18°$ between the external magnetic field and the excitation field in the ZY plane, the excitation field being parallel to the Z axis. Except for the difference in the line intensities and the

orientations of the respective principal axes, the two sets of allowed hf spectra are found to be identical, i.e., they are magnetically inequivalent, but physically equivalent. The angular variations of the spectra for VO^{2+}-doped POM for the orientation of the Zeeman field **B** in the ZX, ZY, and XY planes at liquid-nitrogen temperature (LNT) are displayed in Figs. 4, 5, and 6, respectively. (It should be noted that the excitation field is parallel to the Z axis for the variation of **B** in the ZX and ZY planes, while it is parallel to the X axis for the variation of **B** in the XY plane, at all temperatures.)

The peak-to-peak linewidths of the first-derivative absorption line shapes for the allowed and forbidden-hf-transition lines did not change significantly with temperature.

There are some noteworthy features of the forbidden-hf-transition lines, which occur as singlets for all orientations of the external magnetic field. The intensities of the seven forbidden-hf-transition lines are different from each other. The intensity of the central forbidden line is the largest, while those of the extreme lines are the smallest. The intensities of the outer forbidden-hf-transition lines are not symmetrically distributed with respect to the central line. When the orientation of the external magnetic field is perpendicular to the excitation field, the forbidden-hf-transition lines are not observed. As the angle θ between the orientation of the external magnetic field and that of the excitation field decreases, the intensities of the forbidden-hf-transition lines increase, achieving their maximum when the orientation of the external magnetic field is close to that of the excitation field, but not exactly parallel to it. (For more detail on intensities see Sec. V.) At this orientation, they are even more intense than the allowed-hf-transition lines. The change in intensities of the allowed-hf-transition lines as a function of θ is found to be opposite to that of the forbidden-hf-transition lines, i.e., they are large when those for the forbidden-hf-transition lines are small, and vice versa. The angular variation of the intensities of the forbidden-hf-transition lines and that of the allowed-hf-transition lines for the external-magnetic-field orientation in the XY plane at LNT are displayed in Fig. 7.

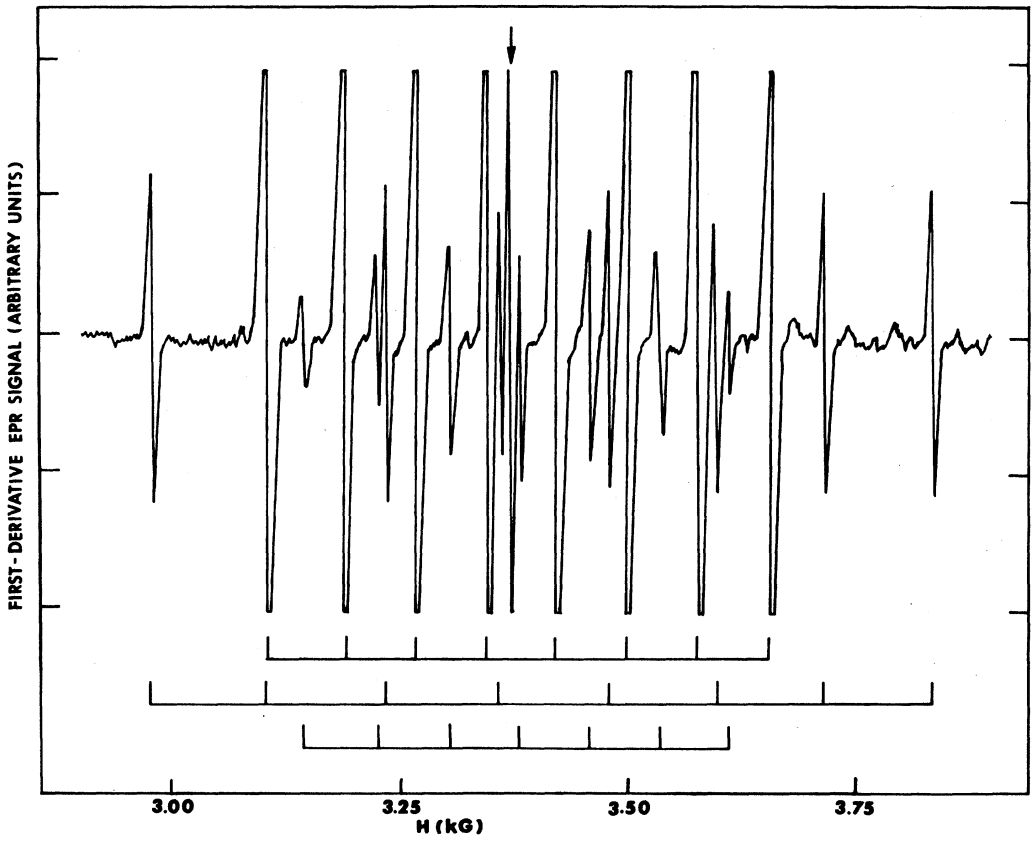

FIG. 3. EPR spectra of VO^{2+} in POM single crystal at 80 K for **B** at 18° from the excitation field in the ZY plane, showing the allowed and forbidden-hf-transition lines. (The orientation of $\mathbf{B}_{ex}$ is along the Z axis.) The first two sets of eight vertical lines below the spectrum indicate the allowed ($\Delta M \pm 1, \Delta m = 0$) transitions for the VO^{2+} complexes, while the lowest one indicates the forbidden ($\Delta M = 1, \Delta m = -1$) transitions. The arrow indicates the 1,1-diphenyl-2-picrylhydrazine (DPPH) resonance signal. (Frequency of the microwave = 9.511 GHz.)

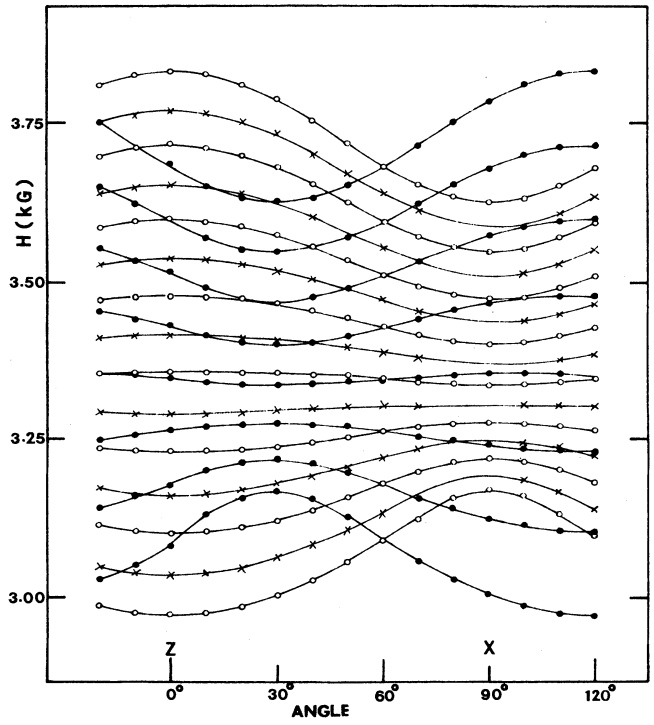

FIG. 4. Angular variation of the EPR line positions observed at 80 K in the ZX plane for VO^{2+}-doped POM. The open and solid circles represent the experimental line positions corresponding to the allowed transitions for the sites I and II, while the crosses represent the forbidden hf transitions corresponding to site I. The continuous lines are smooth curves that connect data points for the same transition. (Frequency=9.462 GHz.)

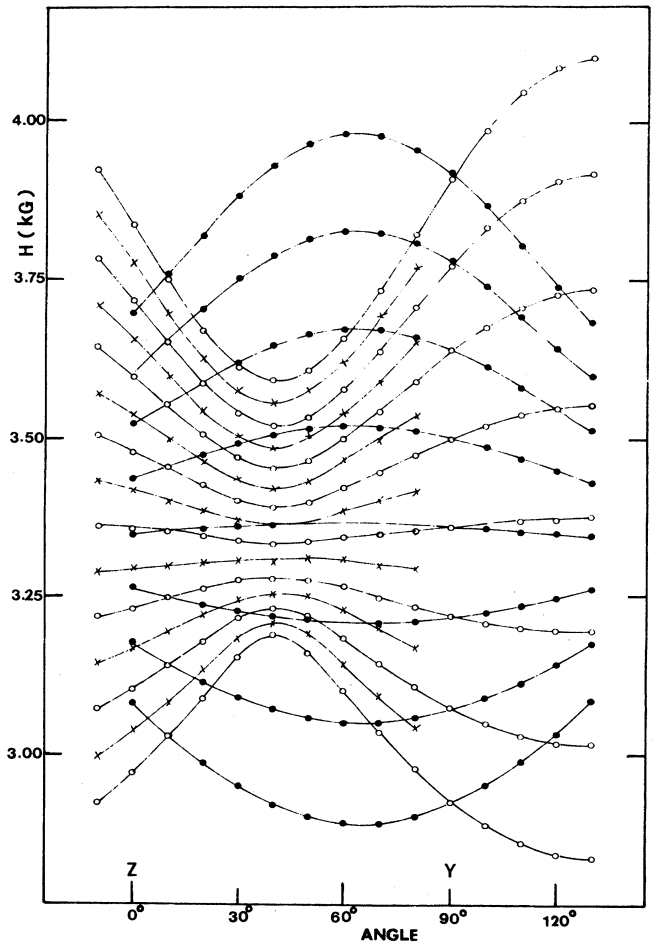

FIG. 5. Angular variation of the EPR line positions observed at 80 K in the ZY plane for VO^{2+}-doped POM. Further details are the same as those expressed in the caption of Fig. 4. (Frequency=9.511 GHz.)

IV. SPIN-HAMILTONIAN PARAMETERS

A. Spin Hamiltonian

VO^{2+} ion consists of a V^{4+} ion ($3d^1$ configuration) and an O^{2-} ion ($2p^6$ configuration). This means that the magnetic moment of the vanadyl ion, VO^{2+}, arises from the single unpaired electron ($3d^1$); thus its electronic spin $S=\frac{1}{2}$. On the other hand, its nuclear spin is that of vanadium nucleus ($^{51}V, I=\frac{7}{2}$). The spin Hamiltonian characterizing VO^{2+} can be expressed as

$$\mathcal{H}=\beta \mathbf{S}\cdot\underline{g}\cdot\mathbf{B}+\mathbf{I}\cdot\underline{A}\cdot\mathbf{S}+\mathbf{I}\cdot\underline{Q}\cdot\mathbf{I}-\beta_N\mathbf{I}\cdot\underline{g}_n\cdot\mathbf{B}\ . \tag{4.1}$$

In Eq. (4.1) β, β_N and $\mathbf{B}$ are, respectively, the Bohr magneton, the nuclear magneton, and the external magnetic field, while $\underline{A}$ and $\underline{Q}$ are, respectively, the hyperfine-interaction matrix and quadrupole-coupling tensor.

B. Evaluation of spin-Hamiltonian parameters

The components of $\underline{g}^2$ and $\underline{A}^2$ tensors were evaluated, for both the strong and weak sets of spectra, by the use of a least-square-fitting (LSF) method, developed by Misra,[11] applicable to noncoincident principal axes of the $\underline{g}^2$ and $\underline{A}^2$ tensors. The components of the $\underline{g}^2$ tensors of the two VO^{2+} complexes were first evaluated by LSF procedures[14] from separate simultaneous fittings of the centers of the sets of allowed-hf-transition line positions (a total of 57 centers for each complex), observed for orientations of the external magnetic field in the orthogonal planes ZX, ZY, and XY. (X, Y, and Z axes were defined earlier.) From the components of the $\underline{g}^2$ tensor, the principal values (and their direction cosines) were calculated by a diagonalization of the $\underline{g}^2$ matrix. These principal values ($g_{X'X'}$, $g_{Y'Y'}$, and $g_{Z'Z'}$) and direction cosines, in conjunction with typical values of the $\underline{A}^2$ tensor, were then used as initial values in a subsequent LS fitting of the various hf-transition line positions using second-order-perturbed eigenvalues. The frame of reference (X', Y', Z'), in which the $\underline{g}^2$ tensor is diagonal,[11] was used to evaluate the 12 parameters: $\underline{g}^2_{X'X'}$, $\underline{g}^2_{Y'Y'}$, $\underline{g}^2_{z'z'}$, α, β, γ, and $\underline{A}^2_{ij}$ ($i,j=X', Y', Z'; i\neq j$). Here α, β, and γ are the Euler angles required to rotate the principal axes of the

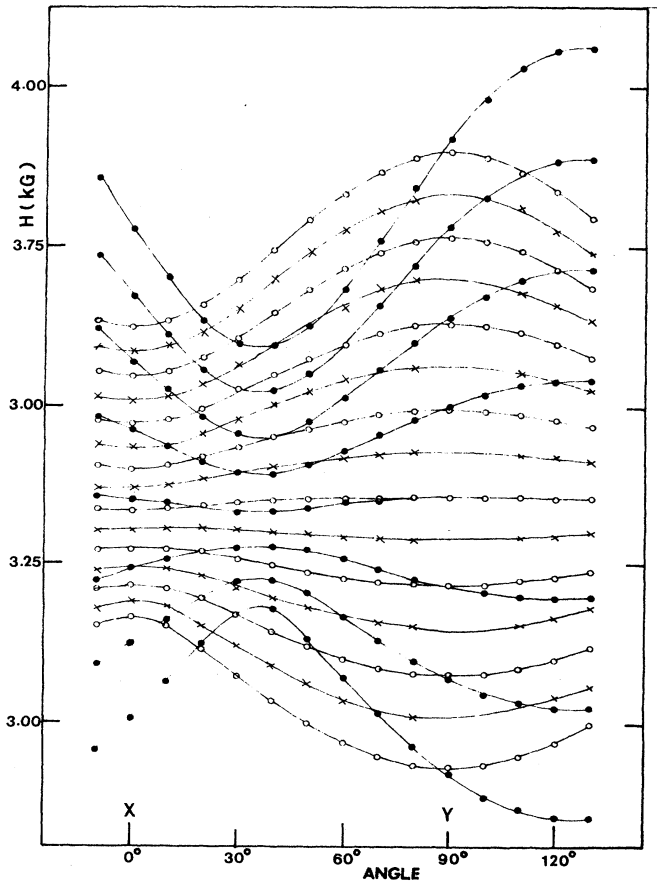

FIG. 6. Angular variation of the EPR line positions observed at 80 K in the XY plane for VO^{2+}-doped POM. Further details are the same as those expressed in the caption of Fig. 4. (Frequency=9.510 GHz.)

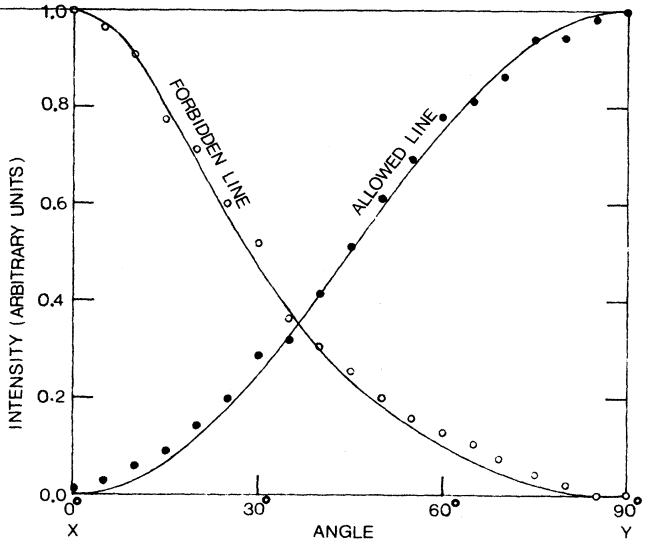

FIG. 7. Angular variation at 80 K of the intensities of the allowed- and forbidden-hf-transition lines for the fourth line (counted in order of increasing **B**) in the XY plane for a VO^{2+}-doped POM single crystal. The empty and solid circles represent the experimental values of the intensities of the forbidden- and the allowed-hf-transition lines, respectively, while the continuous curves represent the calculated values. Both the experimental and theoretical values have been normalized, so that the maximum value of each of these is unity. (Frequency=9.510 GHz.)

$\underline{g}^2$ tensor (X', Y', Z') to coincide with the laboratory axes (X, Y, Z). (Note that tensor $\underline{A}^2$ is symmetric, i.e., $\underline{A}^2_{ij} = \underline{A}^2_{ji}$; thus it is described by six independent elements.) This means that a total of 384 allowed-hf-transition line positions, observed for each of the two VO^{2+} complexes, were fitted simultaneously, in a least-squares fashion, to evaluate these 12 parameters. The principal values of $\underline{g}$ and $\underline{A}$ matrices and their direction cosines at 295, 80, 42, and 4.2 K, so obtained, are listed in Tables I, II, III, and IV, respectively. (The principal values of the $\underline{g}$ and $\underline{A}$ matrices are the square roots of the principal values of the $\underline{g}^2$ and $\underline{A}^2$ tensors respectively; the direction cosines of the $\underline{g}$ and $\underline{A}$ matrices are the same as those of the matrices representing the $\underline{g}^2$ and $\underline{A}^2$ tensors, respectively.[14]) In Tables I–IV, the direction cosines of the $\underline{g}$ matrix are given with respect to the laboratory frame (X, Y, Z) depicted in Fig. 2, while those of the $\underline{A}$ matrix are expressed relative to the principal axes of the $\underline{g}^2$ tensor (X', Y', Z'). The allowed line positions do not depend on tensor $\underline{Q}$ in first-order of perturbation. Thus only the elements of $\underline{g}^2$ and $\underline{A}^2$ tensors have been evaluated from the allowed hf line positions. The elements of the tensor $\underline{Q}$ are evaluated from the forbidden line positions.

It is seen from Tables I–IV that the values of two of the principal g values for any one VO^{2+} complex are quite close to each other, but not exactly equal to each other. This indicates that there is a slight deviation from axial symmetry at VO^{2+} site. This deviation is probably related to the asymmetry in the local environment.[10]

The elements of the $\underline{Q}$ matrix were evaluated from the forbidden-hf-transition line positions (for the more intense set only) using another LSF procedure. Previously determined values of the $\underline{g}^2$ and $\underline{A}^2$ tensors were used as constants; only the components of $\underline{Q}$ were varied. A total of 336 forbidden-hf-transition line positions for external magnetic field orientations in the three mutually perpendicular planes ZX, ZY, and XY were simultaneously fitted in a least-squares procedure; the expressions for the required eigenvalue differences and their derivatives with respect to the components of $\underline{Q}$ are given in Appendix A. The matrix of $\underline{Q}$, so obtained, was diagonalized to obtain the principal values of the $\underline{Q}$ tensor, as well as its direction cosines with respect to the principal axes of the $\underline{g}^2$ tensor. These values are listed in Tables I–IV.

The asymmetry parameter η for the case where $|Q_{x''x''}| \leq |Q_{y''y''}| \leq |Q_{z''z''}|$ can be expressed as[16]

$$\eta = (Q_{x''x''} - Q_{y''y''})/Q_{z''z''} \ . \tag{4.2}$$

TABLE I. The principal values and direction cosines (eigenvectors) of the $\underline{g}$ and $\underline{A}$ matrices and the tensor $\underline{Q}$ of a VO^{2+}-doped POM single crystal at 295 K. The g values are dimensionless, while A and Q values are expressed in units of GHz. The indicated errors are those estimated by the use of a statistical method (Ref. 15). The direction cosines of the $\underline{g}^2$ tensor are given with respect to the laboratory frame (X,Y,Z), defined in Sec. III, and depicted in Fig. 2, while those of both the $\underline{A}^2$ and $\underline{Q}$ tensors are expressed relative to (X',Y',Z'), the principal axes of the $\underline{g}^2$ tensor. The forbidden-hf-transition lines corresponding to site II were too weak to be observed, thus, tensor $\underline{Q}$ could not be determined for site II.

Site I					Site II				
Principal values		Direction cosines			Principal values		Direction cosines		
		Z	X	Y			Z	X	Y
$g_{Z'Z'}=1.944\pm0.001$	Z'	−0.660	0.033	0.750	$g_{Z'Z'}=1.943\pm0.001$	Z'	0.323	−0.632	0.705
$g_{X'X'}=1.981\pm0.002$	X'	0.480	−0.749	0.456	$g_{X'X'}=1.984\pm0.001$	X'	0.464	0.755	0.464
$g_{Y'Y'}=1.983\pm0.001$	Y'	0.577	0.662	0.479	$g_{Y'Y'}=1.978\pm0.001$	Y'	−0.825	0.177	0.537
		X'	Y'	Z'			X'	Y'	Z'
$A_{Z''Z''}=0.483\pm0.001$	Z''	0.034	−0.017	0.999	$A_{Z''Z''}=0.499\pm0.001$	Z''	0.051	0.053	0.997
$A_{X''X''}=0.182\pm0.002$	X''	−0.889	0.456	0.038	$A_{X''X''}=0.181\pm0.001$	X''	−0.923	0.385	0.027
$A_{Y''Y''}=0.149\pm0.002$	Y''	−0.456	−0.890	0.001	$A_{Y''Y''}=0.152\pm0.001$	Y''	−0.383	−0.921	0.069
$Q_{Z''Z''}=0.0022\pm0.001$	Z''	0.988	0.141	−0.059					
$Q_{X''X''}=-0.0007\pm0.001$	X''	−0.153	0.905	−0.397					
$Q_{Y''Y''}=-0.0016\pm0.001$	Y''	−0.003	0.401	0.916					

TABLE II. The principal values and the direction cosines (eigenvectors) of the $\underline{g}$ and $\underline{A}$ matrices and the tensor $\underline{Q}$ at 80 K for a VO^{2+}-doped POM single crystal. For explanation of notations, units, reference axes, and other details, see the caption of Table I.

Site I					Site II				
Principal values		Direction cosines			Principal values		Direction cosines		
		Z	X	Y			Z	X	Y
$g_{Z'Z'}=1.943\pm0.001$	Z'	−0.660	0.034	0.750	$g_{Z'Z'}=1.940\pm0.001$	Z'	0.357	−0.599	0.717
$g_{X'X'}=1.980\pm0.002$	X'	0.480	−0.749	0.456	$g_{X'X'}=1.988\pm0.001$	X'	0.454	0.782	0.427
$g_{Y'Y'}=1.991\pm0.001$	Y'	0.578	0.661	0.479	$g_{Y'Y'}=1.982\pm0.001$	Y'	−0.816	0.173	0.551
		X'	Y'	Z'			X'	Y'	Z'
$A_{Z''Z''}=0.489\pm0.001$	Z''	0.027	−0.014	0.999	$A_{Z''Z''}=0.499\pm0.001$	Z''	0.054	0.044	0.998
$A_{X''X''}=0.182\pm0.002$	X''	−0.892	0.451	0.030	$A_{X''X''}=0.182\pm0.001$	X''	−0.933	0.358	0.034
$A_{Y''Y''}=0.154\pm0.001$	Y''	−0.451	−0.893	−0.001	$A_{Y''Y''}=0.147\pm0.001$	Y''	−0.356	−0.933	0.061
$Q_{Z''Z''}=0.0021\pm0.001$	Z''	0.979	0.081	0.188					
$Q_{X''X''}=-0.0007\pm0.001$	X''	−0.077	0.997	−0.027					
$Q_{Y''Y''}=-0.0014\pm0.001$	Y''	−0.189	0.012	0.982					

TABLE III. The principal values and direction cosines (eigenvectors) of the $\underline{g}$ and $\underline{A}$ matrices and tensor $\underline{Q}$ at 42 K for VO^{2+}-doped POM single crystal. For explanation of notations, units, reference axes, and other details, see the caption of Table I.

Site I						Site II					
Principal values		Direction cosines			Principal values		Direction cosines				
		Z	X	Y			Z	X	Y
$g_{Z'Z'}=1.943\pm0.001$	Z'	−0.660	0.034	0.750	$g_{Z''Z''}=1.934\pm0.001$	Z'	0.326	−0.619	0.715
$g_{X'X'}=1.977\pm0.002$	X'	0.480	−0.749	0.456	$g_{X''X''}=1.984\pm0.001$	X'	0.467	0.763	0.448
$g_{Y'Y'}=1.986\pm0.001$	Y'	0.578	0.661	0.479	$g_{Y''Y''}=1.981\pm0.001$	Y'	−0.822	0.188	0.537
		X'	Y'	Z'			X'	Y'	Z'
$A_{Z''Z''}=0.488\pm0.001$	Z''	0.027	−0.014	0.999	$A_{Z''Z''}=0.506\pm0.001$	Z''	0.053	0.049	0.997
$A_{X''X''}=0.185\pm0.001$	X''	−0.913	0.407	0.030	$A_{X''X''}=0.191\pm0.001$	X''	−0.912	0.409	0.028
$A_{Y''Y''}=0.153\pm0.002$	Y''	−0.407	−0.913	−0.001	$A_{Y''Y''}=0.145\pm0.001$	Y''	−0.407	−0.911	0.066
$Q_{Z''Z''}=0.0020\pm0.001$	Z''	0.983	−0.058	0.174					
$Q_{X''X''}=-0.0004\pm0.001$	X''	0.010	0.964	0.264					
$Q_{Y''Y''}=-0.0016\pm0.001$	Y''	−0.183	−0.258	0.948					

In Eq. (4.2) $Q_{x''x''}$, $Q_{y''y''}$, and $Q_{z''z''}$ are the principal values of the tensor $\underline{Q}$. (Note that $Q_{x''x''}+Q_{y''y''}+Q_{z''z}=0$.) Using the principal values of the tensor $\underline{Q}$ the values of the asymmetry parameter η were calculated to be 0.34, 0.33, 0.56, and 0.60 at 295, 80, 42, and 4.2 K, respectively. This indicates that the asymmetry of the quadrupole tensor increases with decreasing temperature.

It should be noted that although the contribution of the quadrupole interaction to the intensities of the forbidden hf doublets is too small to be significant experimentally, as seen in Sec. V below, the contribution of the quadrupole interaction to the positions of the forbidden lines is, indeed, sufficiently significant to enable determination of the quadrupole tensor components from the observed positions of the forbidden-hf-transition lines.

V. INTENSITIES OF LINES

For a general orientation of the Zeeman field two different sets of eight allowed lines $(\frac{1}{2},m\leftrightarrow-\frac{1}{2},m)$, and seven forbidden singlets $(\frac{1}{2},m\leftrightarrow-\frac{1}{2},m+1)$ are observed for VO^{2+}-doped POM. The intensity expressions for the allowed and forbidden lines are given in Appendix B.

A. Allowed hyperfine lines

As seen in Appendix B, the intensity of the allowed-hf-transition lines is proportional to the transition probability

$$W_{1/2,m\leftrightarrow-1/2,m}=\beta^2B_{\rm ex}^2[{\rm Tr}(\underline{g}^2)-g_1^2](\sin^2\theta)/8\ , \qquad (5.1)$$

where θ is the angle between $\mathbf{B}_{\rm ex}$, the excitation field, and $\mathbf{B}$. The expression inside the square brackets is obviously a function of the orientation of $\mathbf{B}$ with respect to the principal axes of the $\underline{g}^2$, which also depends on θ. However, since the tensor $\underline{g}^2$ is almost isotropic for the present case as seen from Tables I–IV, the expression inside the square brackets in Eq. (5.1) does not depend significantly on θ. In that case, the intensities of the allowed lines vary almost exclusively as $\sin^2\theta$ with the variation of the angle θ between the orientations of the Zeeman field and the excitation field. The observed intensity at LNT of the fourth allowed-hf-transition line (counted in order of increasing $\mathbf{B}$, where the principal values of A are positive) for variation of the Zeeman field $\mathbf{B}$ in the XY plane, is plotted in Fig. 7 as a function of θ. The intensities are normalized such that the intensity is unity for $\theta=90°$. Figure 7 also exhibits a plot of $\sin^2\theta$ (the expected variation); the two appear to be in fairly good agreement; any discrepancy may be ascribed to the slight angular dependence of the expression inside the square bracket in Eq. (5.1) and uncertainty in estimating intensities from the spectra.

B. Forbidden lines

As discussed in Appendix B, the forbidden-hf-transition lines caused by the quadrupole interaction $\mathbf{I}\cdot\underline{Q}\cdot\mathbf{I}$, are seven doublets $(\frac{1}{2},{}^{m}_{m-1}\leftrightarrow-\frac{1}{2},{}^{m-1}_{m}$; $m=\frac{7}{2},\frac{5}{2},\frac{3}{2},$

TABLE IV. The principal values and direction cosines (eigenvectors) of the $\underline{g}$ and $\underline{A}$ matrices and tensor $\underline{Q}$ at 4.2 K for a VO^{2+}-doped POM single crystal. For explanation of notations, units, reference axes, and other details, see the caption of Table I. It should be noted that only the hf lines corresponding to site I were observed; the lines corresponding to site II were too weak to be observed.

Site I				
Principal values		Direction cosines		
		Z	X	Y
$g_{Z'Z'}=1.952\pm0.001$	Z'	−0.660	0.034	0.750
$g_{X'X'}=1.987\pm0.002$	X'	0.481	−0.748	0.457
$g_{Y'Y'}=1.984\pm0.002$	Y'	0.577	0.662	0.478
		X'	Y'	Z'
$A_{Z''Z''}=0.488\pm0.001$	Z''	0.039	−0.009	0.999
$A_{X''X''}=0.181\pm0.002$	X''	−0.891	0.452	0.039
$A_{Y''Y''}=0.157\pm0.001$	Y''	−0.452	−0.892	0.009
$Q_{Z''Z''}=0.0020\pm0.001$	Z''	0.946	0.090	−0.311
$Q_{X''X''}=-0.0004\pm0.001$	X''	0.033	0.929	0.368
$Q_{Y''Y''}=-0.0016\pm0.001$	Y''	0.323	−0.358	0.876

$\frac{1}{2}$, $-\frac{1}{2}$, $-\frac{3}{2}$, and $-\frac{5}{2}$) for VO^{2+}. Their intensities, as calculated from Eq. (B.15) of Appendix B, are in the ratios 21:16:5:0:5:16:21 for any orientation of the Zeeman field with respect to the excitation field. (The two components of any doublet due to the quadrupole interaction have the same intensity.) On the other hand, the hyperfine interaction $\mathbf{I}\cdot\underline{A}\cdot\mathbf{S}$ also produces seven forbidden hf doublets. However, the intensities of the two components of a doublet due to the hf interaction are quite different from each other, as calculated from Eq. (B.14) using the values of the $\underline{g}^2$ and $\underline{A}^2$ tensor components. The intensity of one component is calculated to be anywhere from $\frac{1}{10}$ to $\frac{1}{500}$ that of the other component of the doublet. (Of the two components of the forbidden doublet due to the hf interaction for an *isotropic* $\underline{A}^2$ tensor, the transition probability $W_{1/2,m\leftrightarrow-1/2,m-1}$ is expected to be zero, while the transition probability $W_{1/2,m-1\leftrightarrow-1/2,m}$ is nonzero.) Further, using the fitted values of the $\underline{g}^2$ and $\underline{A}^2$ matrices and the tensor $\underline{Q}$ components, it is seen that the intensities of the forbidden-hf-transition lines caused by the quadrupole interaction are two orders of magnitude smaller than those of the more intense component of the doublet due to the hyperfine interaction. Indeed, the contribution to the intensity of the forbidden hf doublets due to quadrupole interaction, contributing equally to the two components, are negligible. Only singlet forbidden-hf-transition lines are, thus, observed. (There are, of course, contributions to forbidden hf transitions due to cross terms in the hf and quadrupole interactions. However, these are also negligible, compared to those due to purely hf interaction.[1,2])

The angular variation of the intensity of the forbidden-hf-transition lines, as reported in Appendix B, is given by

$$W_{1/2,m\leftrightarrow-1/2,m\pm1}=\beta^2g^2B_{\rm ex}^2[\mathrm{Tr}(\underline{A}^2)-A_1^2\pm2\,\mathrm{Det}(\underline{A})/A][I(I+1)-m(m\pm1)](\cos^2\theta)/[16(\beta gB+Am\pm A/2)^2]\,. \tag{5.2}$$

Here the contribution from the term containing $(g_1^2-g^2)$ in Eq. (B14) has been neglected, because the $\underline{g}^2$ tensor is almost isotropic, and therefore its contribution is negligible. Figure 7 displays the angular variation of the observed and calculated [using Eq. (5.2)] intensities of the fourth forbidden-hf-transition line $(\frac{1}{2},-\frac{1}{2}\leftrightarrow-\frac{1}{2},\frac{1}{2})$ (counted toward increasing **B**) for **B** in the XY plane at *LNT*. Since the determined $\underline{A}^2$ tensor is reasonably anisotropic, the factor in the square bracket in Eq. (5.2) depends significantly on θ, and its maximum value is not necessarily attained at $\theta=0°$. The calculated intensity, therefore, also does not always achieve its maximum value for $\theta=0°$, at which the maximum of the factor $\cos^2\theta$ occurs. In fact, for **B** in the ZX and XY planes and $\mathbf{B}_{\rm ex}$ along the Z and X axes, respectively, the maximum intensity does occur at $\theta=0°$; while for **B** in the ZY plane and $\mathbf{B}_{\rm ex}$ along the Z axis, it occurs at $\theta=20°$.

When the external magnetic field is perpendicular to the excitation field ($\theta=90°$), the probability of the forbidden hf transition due to hf interaction is identically zero, as seen from Eq. (5.2). This has been confirmed experimentally at RT in the present studies.

The relative intensities are calculated via Eq. (5.2) for the orientation of the Zeeman field **B** at 18° from that of the excitation field in the ZY plane, to be 365:664:880:1000:999:845:531 for the set of forbidden hf singlets $(\frac{1}{2},m\leftrightarrow-\frac{1}{2},m+1)$. These are to be compared with the observed relative intensities

420:720:920:1000:960:760:480 at LNT determined from the equation[17]

$$I \propto Y_{\max}(\Delta B_{\text{p.p.}})^2 , \tag{5.3}$$

where $2Y_{\max}$ is the peak-to-peak line height and $\Delta B_{\text{p.p.}}$ is the peak-to-peak linewidth of the first-derivative line shape. The theoretically calculated values can, thus, be deemed to be in reasonably good agreement with those measured experimentally, taking into account the errors in estimating line intensities. It should be noted, from expressions (5.1) and (5.2), that for $\theta=0°$ the intensities of the allowed hf transitions are identically zero, while those of the forbidden hf transitions achieve respective maximum, or close to maximum, values. [As mentioned above, the factor in the square brackets in Eq. (5.2) also depends on θ; thus the maximum of Eq. (5.2) does not occur necessarily at $\theta=0°$.] Experimentally, weakly allowed hf transitions are also observed at $\theta=0°$, because of the existence of residual nonzero component of **B** perpendicular to $\mathbf{B}_{\text{ex}}$. However, the observed forbidden-hf-transition lines (seven singlets) have much larger intensity as compared to that of the allowed-hf-transition lines at $\theta=0°$.

Jain[10] did not observe any forbidden-hf transitions for VO^{2+}-doped POM. This is due to the fact that in his experiment the Zeeman field was always perpendicular to the excitation field, i.e., $\theta=90°$.

VI. POSITIONS OF VO^{2+} IONS IN POM LATTICE

In the spectra only two physically distinct sets of allowed lines, consisting of eight hf-transition lines each, were observed. This indicates that VO^{2+} ions do not substitute for a monovalent K^+ ion; otherwise four sets of eight hf-transition lines should have been observed, because of the presence of four inequivalent K^+ sites in the unit cell of POM. It appears likely that, for charge compensation, the VO^{2+} ion substitutes in place of two nearest-neighbor monovalent K^+ ions in the POM lattice. Thus, it is at an interstitial site, located either in between the four oxygens O(1)-O(2)-O(3)-O(4), or, in between the four oxygens O(1′)-O(2′)-O(3′)-O(4′), as exhibited in Fig. 1. Upon entering the POM lattice, the ligand oxygens coordinate with the VO^{2+} ion to form the $VO(CO_2)_2$ complex. Finally, V—O bonds orient themselves appropriately, to satisfy the requirement of charge compensation.

For any VO^{2+} complex, the orientation of the principal Z axis of the $\underline{g}^2$ tensor is expected to be along the V—O bond.[10,18] Comparing direction cosines of the principal Z axes (obtained from the present EPR data) with those of the lines joining the various pairs formed by the nearest-neighbor ions (calculated from the POM crystal-structure data), it is found that the V—O orientation for site II is along the $K_{(1)}^+$-$K_{(2)}^+$ direction, while the V—O orientation for site I coincides with the quasitwofold axis of the distorted coordination octahedron formed by four oxygen molecules and two water molecules, as indicated in Fig. 1. The angle between the orientations of the two VO^{2+} complexes is 73.2°, as determined from the orientations of the Z axes corresponding to the two sets of EPR spectra at RT. The orientations of the principal Z axes of the $\underline{g}^2$ tensor of VO^{2+}-doped POM single crystal are close to those of a Cu^{2+}-doped POM single crystal,[19] where the Cu^{2+} ions enter the POM lattice interstitially in the same way as do the VO^{2+} ions.

VII. SUPERHYPERFINE INTERACTION

Figure 8 displays the EPR spectra observed at RT for rotation of the sample in the ZY plane. (The forbidden-hf-transition lines were not observed because the orientation of the external magnetic field and the excitation field were maintained perpendicular to each other.) The EPR lines became wider while the peak-to-peak height of the hf-transition lines became smaller as the orientation of the external magnetic field got closer to the direction of the crystallographic c axis. This is attributed to the weak superhyperfine interaction of the paramagnetic ion VO^{2+} with the protons of the nearest water molecules. Abragam and Bleaney[20] suggested that, in general, the superhyperfine structure has axial symmetry about the bond axis, i.e., in the present case, the line connecting the center of the ligands (protons of neighboring H_2O molecules) with that of the magnetic ion (VO^{2+}). The maximum superhyperfine splitting in the present studies is along the bond axis. This unresolved superhyperfine splitting only results in broadening the lines. The maximum linewidth is observed along the crystallographic c axis which makes an angle of 20° with the orientation of the principal Z axis of the $\underline{g}^2$ tensor for site I; it is consistent with the assumption that the principal Z axis of the $\underline{g}^2$ tensor for site I is along the quasitwofold axis of the distorted coordination octahedron, shown in Fig. 1.[19]

Similar observations for the VO^{2+} complex belonging to site II could not be made because of the rather weak intensity of the corresponding spectrum.

VIII. CONCLUSIONS

The following conclusions are drawn from the present EPR study of a VO^{2+}-doped POM crystal.

(i) The observation of singlet forbidden hf transitions, and the angular variation of their intensities, for VO^{2+}-doped POM single crystal, have been explained to result from the external magnetic field having a nonzero component parallel to the excitation field.

(ii) The principal values of the $\underline{g}^2$ and $\underline{A}^2$ tensors and their direction cosines have been evaluated from the positions of the allowed EPR lines, whereas the principal values and the direction cosines of the principal axes of the tensor $\underline{Q}$ have been evaluated from the forbidden-transition line positions.

(iii) A VO^{2+} ion substitutes interstitially for two potassium ions, upon entering the POM lattice.

(iv) The presence of superhyperfine interaction, between VO^{2+} and the protons of H_2O molecules, although not clearly resolved, has been found to cause extra broadening of the lines for the orientations of the external magnetic field close to the crystallographic c axis.

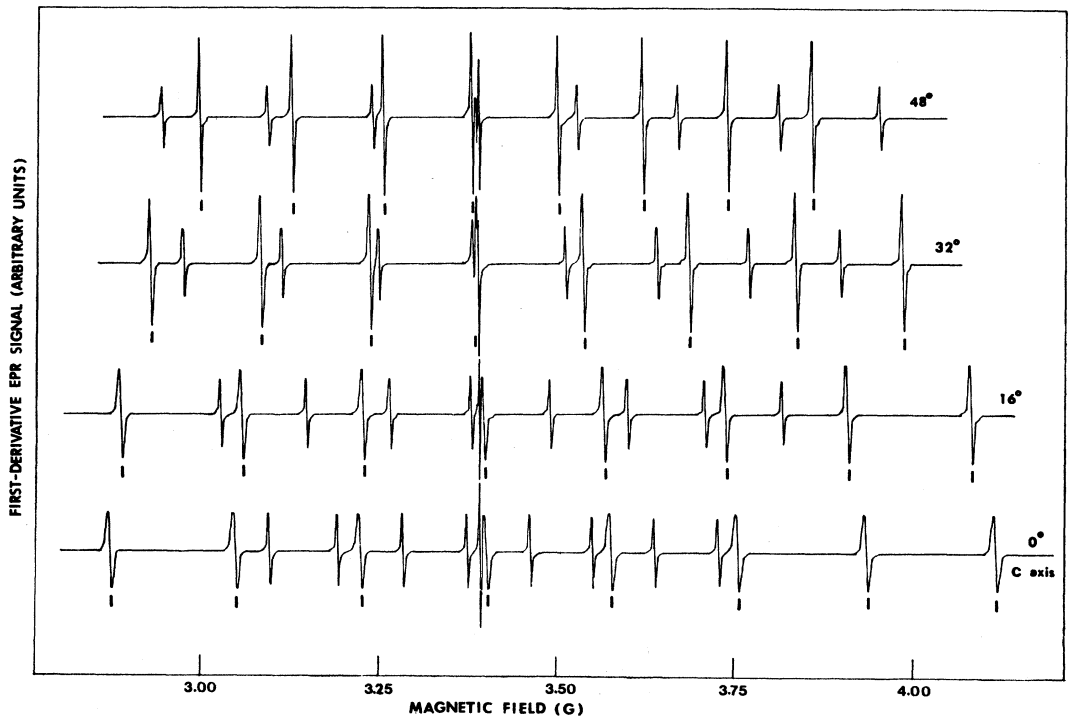

FIG. 8. EPR spectra for a VO^{2+}-doped POM single crystal, as observed for rotation of the crystal in the ZY plane, at RT. The EPR lines for site I (indicated by I) become wider, while the peak-to-peak height of the lines become smaller as the orientation of the external magnetic field gets closer to the direction of the crystallographic c axis. Forbidden-hf-transition lines could not be observed, because the external magnetic field was kept perpendicular to the excitation field in this experiment. (Frequency=9.535 GHz.)

(v) The asymmetry parameter η increases with decreasing temperature.

ACKNOWLEDGMENTS

The authors are grateful to the Natural Sciences and Engineering Research Council of Canada for financial support (Grant No. A4485) and to the Concordia University Computer Center for providing their facilities to analyze the data.

APPENDIX A: EVALUATION OF THE COMPONENTS OF TENSOR $\underline{Q}$

The procedure of evaluating the components of the quadrupole tensor $\underline{Q}$ from forbidden EPR line positions is similar to that for calculating the components of the $\underline{g}^2$ and $\underline{A}^2$ tensors from the allowed line positions,[14] the difference being in the expressions for the eigenvalue differences (which depend on the components of the tensor $\underline{Q}$) between the pair of energy levels participating in resonance and their first and second derivatives with respect to the components of $\underline{Q}$. The details are given in this Appendix.

The second-order perturbed energies, taking into account only the electronic-Zeeman ($\beta \mathbf{S} \cdot \underline{g} \cdot \mathbf{B}$) and hf-interaction ($\mathbf{I} \cdot \underline{A} \cdot \mathbf{S}$) terms valid for $S=\frac{1}{2}$, can be expressed as follows:[13]

$$\begin{aligned} E_{Z,\mathrm{hf}} &= \beta g B M + A M m \\ &\quad + (2\beta g B)^{-1}\{[\mathrm{Tr}(\underline{A}^2) - A_1^2] M [I(I+1) - m^2]/2 \\ &\quad - \mathrm{Det}(\underline{A}) m/(2A) \\ &\quad + (A_1^2 - A^2) M m^2\} \ . \end{aligned} \tag{A1}$$

In Eq. (A1),

$$\begin{aligned} \eta &= \mathbf{B}/|\mathbf{B}| \ , \\ g^2 &= \eta^T \cdot \underline{g}^T \cdot \underline{g} \cdot \eta \ , \\ g^2 A^2 &= \eta^T \cdot \underline{g}^T \cdot \underline{A}^T \cdot \underline{A} \cdot \underline{g} \cdot \eta \ , \\ g^2 A^2 A_1^2 &= \eta^T \cdot \underline{g}^T \cdot \underline{A}^T \cdot \underline{A} \cdot \underline{A}^T \cdot \underline{A} \cdot \underline{g} \cdot \eta \ . \end{aligned} \tag{A2}$$

In Eq. (A2) the superscript T denotes the transpose of a matrix. The quadrupole term $\mathcal{H}_Q$ ($=\mathbf{I} \cdot \underline{Q} \cdot \mathbf{I}$) can be written as follows:

$$\begin{aligned} \mathcal{H}_Q &= Q_{xx}(I_x^2 - I_z^2) + Q_{yy}(I_y^2 - I_z^2) \\ &\quad + Q_{xy}(I_x I_y + I_y I_x) + Q_{yz}(I_y I_z + I_z I_y) \\ &\quad + Q_{xz}(I_x I_z + I_z I_x) \ . \end{aligned} \tag{A3}$$

In writing Eq. (A3) the fact that $\mathrm{Tr}(\underline{Q})=0$ [i.e., $Q_{zz} = -(Q_{xx} + Q_{yy})$] has been taken into account. [This

means that there are only five independent components of the symmetric tensor $\underline{Q}$: Q_{xx}, Q_{yy}, and Q_{ij} $(i,j=x,y,z;\ i\neq j)$, with $Q_{ij}=Q_{ji}$.]

If one transforms $\mathcal{H}_Q$ to the principal-axes system (X',Y',Z') of the $\underline{g}^2$ tensor where the Z' axis has the direction cosines $(a_x/g, a_y/g, a_z/g)$, then I_x contributes a component $I_{z'}$ with the coefficient a_x/g, while I_y and I_z contribute the components $I_{z'}$ with the coefficients a_y/g and a_z/g, respectively. In the principal-axes system (X',Y',Z'), in which the $\underline{g}$ matrix is diagonal $a_x=l'g'_x/g$, $a_y=m'g'_y/g$, and $a_z=n'g'_z/g$, where g'_x, g'_y, and g'_z are the principal values of $\underline{g}$ matrix, and l', m', n' are the direction cosines of the external magnetic field with respect to the principal-axes system (X',Y',Z'), Explicitly.

$$\begin{aligned} l' &= l\cos(X,X')+m\cos(Y,X')+n\cos(Z,X')\ ,\\ m' &= l\cos(X,Y')+m\cos(Y,Y')+n\cos(Z,Y')\ ,\\ n' &= l\cos(X,Z')+m\cos(Y,Z')+n\cos(Z,Z')\ . \end{aligned} \tag{A4}$$

Then in the coordinate system (X',Y',Z'), one has

$$\begin{aligned} \mathcal{H}_Q = I_{z'}^2[&Q_{xx}(a_x^2-a_y^2)+Q_{yy}(a_y^2-a_z^2)+2Q_{xy}a_xa_y\\ &+2Q_{yz}a_ya_z+2Q_{xz}a_xa_z]/g^2\\ &+(\text{terms in } I_{x'}^2 \text{ and } I_{y'}^2)\ . \end{aligned} \tag{A5}$$

After neglecting the terms in $I_{x'}^2$ and $I_{y'}^2$, the contribution of $\mathcal{H}_Q$ to the energy can be expressed as

$$E_Q(m)=Q_0m^2\ , \tag{A6}$$

where,

$$\begin{aligned} Q_0=[&Q_{xx}(a_x^2-a_z^2)+Q_{yy}(a_y^2-a_z^2)\\ &+2Q_{xy}a_xa_y+2Q_{yz}a_ya_z+2Q_{xz}a_xa_z]/g^2\ , \end{aligned} \tag{A7}$$

and m is the nuclear magnetic quantum number. Finally, taking into account the electronic-Zeeman, hyperfine, and nuclear-quadrupole interactions, the energy can be written as follows:

$$E(M,m)=E_{Z,\mathrm{hf}}+Q_0m^2\ . \tag{A8}$$

For the hf-forbidden transition $\frac{1}{2},m-1\leftrightarrow-\frac{1}{2},m$, the energy difference is

$$\begin{aligned} \Delta E=\beta gB+(m-\tfrac{1}{2})A+(2\beta gB)^{-1}\{&[\mathrm{Tr}(\underline{A}^2)-A_1^2][2I(I+1)-2m^2+2m-1]/4\\ &+\mathrm{Det}(A)/(2A)+(A_1^2-A^2)(m^2-m+\tfrac{1}{2})\}-(2m-1)Q_0\ . \end{aligned} \tag{A9}$$

From Eqs. (A9) and (A7), the first derivatives with respect to the components of $\underline{Q}$ can be expressed as follows:

$$\begin{aligned} \partial|\Delta E|/\partial Q_{ij}&=2(2m-1)a_ia_j/g^2 \quad (i,j=x,y,z;i\neq j)\\ \partial|\Delta E|/\partial Q_{ii}&=(2m-1)(a_i^2-a_z^2)/g^2 \quad (i=x,y)\ . \end{aligned} \tag{A10}$$

As for the second derivatives of $|\Delta E|$ with respect to the components of $\underline{Q}$, they are all found to be identically equal to zero, as can be seen from Eq. (A7).

APPENDIX B: CALCULATION OF TRANSITION PROBABILITY

The calculation of transition probabilities, to which the intensities of lines are directly proportional, requires the perturbed eigenfunctions, which are dependent upon the spin Hamiltonian. The following discussion is a generalization of the results given by Rockenbauer and Simon.[21]

Spin Hamiltonian and the perturbed eigenfunctions

The spin Hamiltonian for VO^{2+} ion in POM single crystal is given by Eq. (4.1). In order to obtain the most convenient form of the spin Hamiltonian for perturbation calculation, two special frames of reference (X_1,Y_1,Z_1) and (X_2,Y_2,Z_2) are introduced. The axes Z_1 and Z_2 are chosen to be parallel to the vectors $\underline{g}\cdot\mathbf{B}$ and $\underline{A}\cdot\underline{g}\cdot\mathbf{B}$, respectively; they serve as the quantization axes for the electronic spin **S** and the nuclear spin **I**. The choices of the axes X_1, Y_1, X_2, and Y_2 are arbitrary, as long as (X_1,Y_1,Z_1) and (X_2,Y_2,Z_2) represent two sets of right-handed Cartesian axes. The transformations of **S** and **I** from the laboratory axes (X,Y,Z) to **S'** in the (X_1,Y_1,Z_1) and to **I''** in the (X_2,Y_2,Z_2), axes are represented by the real unitary matrices T' and T'', respectively

$$\mathbf{S}=\underline{T}'\cdot\mathbf{S}' \text{ and } \mathbf{I}=\underline{T}''\cdot\mathbf{I}''\ . \tag{B1}$$

By the use of the transformation matrices $\underline{T}'$ and $\underline{T}''$ the spin Hamiltonian becomes[21]

$$\mathcal{H}=\mathcal{H}^0+\mathcal{H}'_{\mathrm{hf}}+\mathcal{H}'_Q\ , \tag{B2}$$

where

$$\mathcal{H}^0=\beta gBS'_z+AS'_zI''_z\ , \tag{B3}$$

$$\begin{aligned} \mathcal{H}'_{\mathrm{hf}}=&\tfrac{1}{2}(T''_3\cdot\underline{A}\cdot T'_-)S'_+I''_z+\tfrac{1}{2}(T''_3\underline{A}\cdot T'_+)S'_-I''_z\\ &+\tfrac{1}{4}(T''_-\cdot\underline{A}\cdot T'_-)S'_+I''_+ +\tfrac{1}{4}(T''_+\cdot\underline{A}\cdot T'_+)S'_-I''_-\\ &+\tfrac{1}{4}(T''_+\cdot\underline{A}\cdot T'_-)S'_+I''_- +\tfrac{1}{4}(T''_-\cdot\underline{A}\cdot T'_+)S'_-I''_+\ , \end{aligned} \tag{B4}$$

$$\begin{aligned} \mathcal{H}'_Q=&\tfrac{1}{2}Q_1^2[3I_z''^2-I(I+1)]+\tfrac{1}{4}(T''_-\cdot\underline{Q}\cdot T''_-)I''^2_+\\ &+\tfrac{1}{4}(T''_+\cdot\underline{Q}\cdot T''_+)I''^2_-\\ &+\tfrac{1}{2}(T''_-\cdot\underline{Q}\cdot T''_3)(I''_+I''_z+I''_zI''_+)\\ &+\tfrac{1}{2}(T''_+\cdot\underline{Q}\cdot T''_3)(I''_-I''_z+I''_zI''_-)\ . \end{aligned} \tag{B5}$$

In Eqs. (B3), (B4), and (B5)

$$I''_{\pm}=I''_X+iI''_Y,\quad S'_{\pm}=S'_X\pm iS'_Y\ ,$$
$$T'_{\pm}=T'_1\pm iT'_2,\quad T''_{\pm}=T''_1\pm iT''_2\ ,$$

and

$$g^2A^2Q_1^2=\eta^T\cdot\underline{g}^T\cdot\underline{A}^T\cdot\underline{Q}\cdot\underline{A}\cdot\underline{g}\cdot\eta\ , \tag{B6}$$

while η, g, A, and superscript T have already been defined in Appendix A. In Eqs. (B4)–(B6) T'_1 and T'_2 and T'_3 are the first, second, and third rows of T', respectively. Corresponding to X, Y, and Z components, T''_1, T''_2, and T''_3 are similarly defined.

Consider now $\mathcal{H}^0$ as given by Eq. (B3) to be the zero-order Hamiltonian, whose eigenfunctions and eigenvalues are $|M,m\rangle^0$ and $E^0_{M,m}$. Thus

$$\mathcal{H}^0|M,m\rangle^0=E^0_{M,m}|M,n\rangle^0\ , \tag{B7}$$

where $E^0_{M,m}=\beta gBM+AMm$. $\mathcal{H}'=\mathcal{H}'_{\rm hf}+\mathcal{H}'_Q$ is now treated as perturbation; $\mathcal{H}'_{\rm hf}$ and $\mathcal{H}'_Q$ as given by (B4) and (B5) are perturbations due to the hyperfine and quadrupole interactions, respectively.

The perturbed eigenfunction to first order can be written as

$$|M,m\rangle=|M,m\rangle^0+\sum_{M',m'}{}'\frac{(|M',m'\rangle^{00}\langle M',m'|\mathcal{H}'|M,m\rangle^0)}{(E^0_{M,m}-E^0_{M',m'})}\ . \tag{B8}$$

The prime on the summation sign in Eq. (B8) means that $M',m'=M,m$ is omitted in the summation.

Transition probability

The time-dependent perturbation Hamiltonian due to a microwave excitation field is

$$\mathcal{H}_{\rm ex}(t)=\beta\mathbf{S}\cdot\underline{g}\cdot\mathbf{B}_{\rm ex}\cos(2\pi\nu t)\ , \tag{B9}$$

where $B_{\rm ex}$ and ν stand for the amplitude and frequency of the excitation field, respectively. According to the time-dependent perturbation theory the first-order-transition probability at resonance, for the transition $M,m\leftrightarrow M',m'$, is

$$W_{M,m\leftrightarrow M',m'}=|\langle M,m|\beta\mathbf{S}\cdot\underline{g}\cdot\mathbf{B}_{\rm ex}|M',m'\rangle|^2\ . \tag{B10}$$

For the present calculations, the direction of the excitation field is chosen to be arbitrary at an angle θ to the Zeeman field $\mathbf{B}$. Applying the transformation T', introduced earlier, one has

$$\mathbf{S}\cdot\underline{g}\cdot\mathbf{B}_{\rm ex}=B_{\rm ex}[gS'_z\cos\theta+\tfrac{1}{2}(T'_-\cdot\underline{g}\cdot\eta')S'_+\sin\theta+\tfrac{1}{2}(T'_+\cdot\underline{g}\cdot\eta')S'_-\sin\theta+(T'_3\cdot\underline{g}\cdot\eta')S'_z\sin\theta]\ , \tag{B11}$$

where η' is a unit vector, perpendicular to the Zeeman field $\mathbf{B}$, lying in the plane containing $\mathbf{B}$ and $\mathbf{B}_{\rm ex}$.

Allowed transitions

The contributions to the allowed-transition probability from the first and fourth terms containing S'_z of Eq. (B11) are negligible, compared to those from the second and third terms, containing S'_+ and S'_-. This can be seen by comparing the relevant matrix elements of S'_z and S'_+, S'_- for the transitions $\frac{1}{2},m\leftrightarrow-\frac{1}{2},m$. Using the contributions from the second and third terms and considering only the leading term of Eq. (B8), the probability for the allowed hf transitions is, finally, obtained to be[21]

$$W_{1/2,m\leftrightarrow-1/2,m}=\beta^2B_{\rm ex}^2[{\rm Tr}(\underline{g}^2)-g_1^2](\sin^2\theta)/8\ , \tag{B12}$$

where

$$g^2g_1^2=\eta^T\cdot\underline{g}^T\cdot\underline{g}\cdot\underline{g}^T\cdot\underline{g}\cdot\eta\ ,$$

and

$${\rm Tr}(\underline{g}^2)=(\underline{g}^T\cdot\underline{g})_{xx}+(\underline{g}^T\cdot\underline{g})_{yy}+(\underline{g}^T\cdot\underline{g})_{zz}\ . \tag{B13}$$

It is seen from Eq. (B12) that the probability for the allowed transitions $W_{1/2,m\leftrightarrow-1/2,m}$ is nonzero only when the microwave excitation field $\mathbf{B}_{\rm ex}$ has a nonzero component perpendicular to $\mathbf{B}$.

Forbidden hyperfine transitions

If $\mathcal{H}'_Q\ll\mathcal{H}'_{\rm hf}$, as judged in terms of their matrix elements, the forbidden transitions $(\frac{1}{2},m\leftrightarrow-\frac{1}{2},m\pm1)$ are predominantly due to the hf interaction, and one can approximate $\mathcal{H}'=\mathcal{H}'_{\rm hf}$ in Eq. (B8) for the calculation of perturbed wave functions. In that case, one has for the probability of the forbidden hf transitions $\frac{1}{2},m\leftrightarrow-\frac{1}{2},m\pm1$

$$W_{1/2,m\leftrightarrow-1/2,m\pm1}=\beta^2B_{\rm ex}^2[{\rm Tr}(\underline{A}^2)-A_1^2\pm2\,{\rm Det}(\underline{A})/A]\times[I(I+1)-m(m\pm1)][2g^2\cos^2\theta+(g_1^2-g^2)\sin^2\theta]/32(\beta gB+Am\pm A/2)^2\ , \tag{B14}$$

where

$${\rm Tr}(\underline{A}^2)=(\underline{A}^2)_{xx}+(\underline{A}^2)_{yy}+(\underline{A}^2)_{zz}\ ,$$

while A_1^2 has already been defined in Appendix A [Eq. (A2)].

It is seen from Eq. (B14) that for an isotropic $\underline{g}^2$ tensor, which implies $(g_1^2-g^2)=0$, the probability for the forbidden transition, $W_{1/2,m\leftrightarrow-1/2,\pm1}$ is nonzero when $\theta\neq90°$, i.e., there is a nonzero component of $\mathbf{B}_{\rm ex}$ parallel to $\mathbf{B}$. Equation

(B14) is a generalization of the expression given by Rockenbauer and Simon[21] for the special case $\theta=90°$ to an arbitrary value of θ.

On the other hand, the contribution of $\mathcal{H}'_Q$ alone to the transition probability for the forbidden hf transitions is

$$W_{1/2,m\leftrightarrow -1/2,m\pm 1}=\beta^2 B_{\rm ex}^2[{\rm Tr}(\underline{g}^2)-g_1^2](Q_2^2-Q_1^4)[I(I+1)-m(m\pm 1)](2m\pm 1)^2(\sin^2\theta)/2A^2 , \tag{B15}$$

where

$$g^2A^2Q_2^2=\boldsymbol{\eta}^T\cdot\underline{g}^T\cdot\underline{A}^T\cdot\underline{Q}^T\cdot\underline{Q}\cdot\underline{A}\cdot\underline{g}\cdot\boldsymbol{\eta} . \tag{B16}$$

Equation (B15) is, again, a generalization of the result given by Rockenbauer and Simon,[21] for the particular case $\theta=90°$, to an arbitrary value of θ.

---

*Permanant address: Physics Department, Jilin University, Jilin, People's Republic of China.

[1]S. K. Misra and G. C. Upreti, Magn. Reson. Rev. **12**, 1 (1987).

[2]S. K. Misra and G. C. Upreti, in *Electronic Magnetic Resonance of the Solid State,* edited by J. Weil (Canadian Society for Chemistry, Ottawa, 1987), p. 69.

[3]R. L. Belford, D. T. Huang, and H. So, Chem. Phys. Lett. **14**, 592 (1972).

[4]M. A. Hitchman and R. L. Belford, Inorg. Chem. **8**, 958 (1969).

[5]M. A. Hitchman, B. W. Moores, and R. L. Belford, Inorg. Chem. **8**, 1817 (1969).

[6]S. R. P. Smith, P. V. Auzins, and J. E. Wertz, Phys. Rev. **166**, 222 (1968).

[7]P. A. Narayana, J. Chem. Phys. **55**, 4283 (1971).

[8]P. A. Narayana and K. V. L. N. Sastry, J. Chem. Phys. **54**, 2281 (1971).

[9]V. P. Chacko and P. T. Manoharan, J. Magn. Reson. **22**, 7 (1976).

[10]V. K. Jain, Phys. Status Solidi B **97**, 337 (1980).

[11]S. K. Misra, Physica **151B**, 433 (1988); Arab. J. Sci. Eng. **13**, 255 (1988).

[12]A Sequera, S. Srikanta, and R. Chidambaran, Acta Crystallogr. Sect. B **26**, 77 (1970).

[13]B. Pedersen and D. F. Holcomb, J. Chem. Phys. **38**, 61 (1963).

[14]S. K. Misra, Physica **124B**, 53 (1983); S. K. Misra, G. Bandet, G. Bacquet, and T. E. McEnally, Phys. Status Solidi A **80**, 581 (1983).

[15]S. K. Misra and S. Subramanian, J. Phys. C **15**, 7199 (1982).

[16]C. P. Poole, Jr. and H. A. Farach, *The Theory of Magnetic Resonance* (Wiley, New York, 1972).

[17]J. E. Wertz and J. R. Bolton, *Electron Spin Resonance-Elementary Theory and Practical Applications* (McGraw-Hill, New York, 1972).

[18]R. H. Borcherts and C. Kikuchi, J. Chem. Phys. **40**, 2270 (1964).

[19]V. M. Vinokurov, G. R. Bulka, N. M. Gainullina, and N. M. Nizamutinov, Kristallografiya **21**, 766 (1976) [Sov. Phys. Crystallogr. **21**, 434 (1976)].

[20]A. Abragam and B. Bleaney, *Electron Paramagnetic Resonance of Transition Ions* (Clarendon, Oxford, 1970).

[21]A. Rockenbauer and P. Simon, Mol. Phys. **28**, 1113 (1974).